Development of hydrocephalus in mice lacking SOCS7

Danielle L. Krebs*, Donald Metcalf*, Tobias D. Merson*, Anne K. Voss*, Tim Thomas*, Jian-Guo Zhang*, Steven Rakar*, Moira K. O'Bryan†, Tracy A. Willson*, Elizabeth M. Viney*, Lisa A. Mielke*, Nicos A. Nicola*, Douglas J. Hilton*, and Warren S. Alexander*‡

*The Walter and Eliza Hall Institute of Medical Research, 1G Royal Parade, Parkville, Victoria 3050, Australia; and †Monash Institute of Reproduction and Development, Monash University, Clayton, Victoria 3168, Australia

Contributed by Donald Metcalf, September 16, 2004

SOCS7 is a member of the suppressor of cytokine signaling (SOCS) family of proteins (SOCS1-SOCS7 and CIS). SOCS proteins are composed of an N-terminal domain of variable length, a central Src homology 2 domain, and a C-terminal SOCS box. Biochemical and genetic studies have revealed that SOCS1, SOCS2, SOCS3, and CIS play an important role in the termination of cytokine and growth factor signaling. However, the biological actions of other SOCS proteins are less well defined. To investigate the physiological role of SOCS7, we have used gene targeting to generate mice that lack expression of the *Socs7* gene. *Socs7*$^{-/-}$ mice were born in expected numbers, were fertile, and did not exhibit defects in hematopoiesis or circulating glucose or insulin concentrations. However, *Socs7*$^{-/-}$ mice were 7–10% smaller than their wild-type littermates, and within 15 weeks of age ≈50% of the *Socs7*$^{-/-}$ mice died as a result of hydrocephalus that was characterized by cranial distortion, dilation of the ventricular system, reduced thickness of the cerebral cortex, and disorganization of the subcommissural organ. *In situ* hybridization studies revealed prominent expression of *Socs7* in the brain, suggestive of an important functional role of SOCS7 in this organ.

SOCS7 is a member of the suppressor of cytokine signaling (SOCS) family, which consists of eight proteins, SOCS1–SOCS7 and CIS. SOCS family members contain an N-terminal domain of variable length, a central Src homology 2 (SH2) domain, and a 40-aa motif at the C terminus termed the SOCS box (1). CIS and SOCS1–SOCS3 are potent feedback inhibitors of cytokines regulated by the Janus family of tyrosine kinases (JAKs) and the signal transducers and activators of transcription (STATs) (1, 2). Comparatively little is known about the actions of SOCS4–SOCS7.

At the primary amino acid level, SOCS7 is most homologous to SOCS6, the two proteins exhibiting 56% amino acid identity within the SH2 domains and 53% within the SOCS box. The N-terminal domains of SOCS6 and SOCS7 exceed 350 aa in length, and whereas the SOCS6 N-terminal domain contains no identifiable protein interaction motifs, the SOCS7 N-terminal domain contains a putative nuclear localization signal and six proline-rich regions (3). Homology within the SOCS6 and SOCS7 SH2 domains extends to binding specificity, in that both SH2 domains preferentially bind to phosphopeptides containing a valine in the phosphotyrosine (pY) +1 position and a hydrophobic residue in the pY +2 and pY +3 positions (4). The primary structural similarity and the shared phosphopeptide-binding specificity raise the possibility that SOCS6 and SOCS7 might share at least some biochemical and biological actions.

Several lines of evidence suggest that SOCS6 and SOCS7 might regulate insulin signaling. The SOCS6 and SOCS7 SH2 domains bind to insulin receptor substrate 2 (IRS-2), IRS-4, and the p85 subunit of phosphatidylinositol-3 kinase (PI3K), proteins that play an important role in insulin-induced signaling (4). Overexpressed versions of SOCS6 have been reported to bind to the insulin receptor (IR) in response to insulin treatment and to inhibit the insulin dependent activation of Akt, Erk1/2, and IRS-1 (5). Paradoxically, however, transgenic mice overexpressing SOCS6 displayed enhanced insulin-dependent Akt activation with increased insulin sensitivity and enhanced glucose metabolism (6). When mice lacking SOCS6 were subjected to an insulin or glucose challenge, their ability to clear glucose was indistinguishable from that of their wild-type counterparts, suggesting that alone, SOCS6 is not essential for appropriate insulin signaling (4).

SOCS6 and SOCS7 have also been implicated in the regulation of other receptor tyrosine kinases. Ectopically expressed versions of SOCS6 interact with c-Kit in an SH2 domain-dependent manner, resulting in inhibition of stem cell factor (SCF)-induced proliferation, as well as SCF-induced activation of Erk1/2 and p38 (7). In addition, the proline-rich N-terminal region of SOCS7 binds to vinexin, Nck, Ash, and phospholipase Cγ, and the SOCS7 SH2 domain binds to the tyrosine phosphorylated epidermal growth factor receptor (3, 8). These findings suggest that SOCS6 and SOCS7 could potentially be involved in the regulation of a diverse range of signal transduction pathways.

With the aim of uncovering the biological action of SOCS7, we have used gene targeting to disrupt the *Socs7* gene in mice. Although *Socs7*$^{-/-}$ mice were born in apparent good health, approximately half developed hydrocephalus and died within 15 weeks of age. This observation, together with the finding that *Socs7* is prominently expressed in murine brain, suggests that SOCS7 may be required for the maintenance of normal cerebrospinal fluid homeostasis.

Materials and Methods

Generation of Targeted ES Cells and *Socs7*$^{-/-}$ Mice. The murine *Socs7* locus spans >31 kb and contains at least 10 exons (Fig. 1*A*). 4.1-kb 5′ and 4.0-kb 3′ arms from the murine *Socs7* gene were amplified by PCR and cloned into a plasmid containing a lacZ gene and PGK-neo resistance cassette (Fig. 1*A*). This targeting vector, which was designed to delete four exons encoding the C-terminal 114 aa of the SOCS7 N-terminal domain as well as 56 aa of the SH2 domain, was linearized and electroporated into C57BL/6-derived embryonic stem (ES) cells (9). Southern blots of *Eco*RI-digested genomic DNA probed with a 450-bp genomic *Socs7* fragment located 3′ to the targeting vector (3′ probe, Fig. 1*A*) revealed that 4 of 528 clones surviving selection in 175 μg/ml G418 contained an appropriate recombination at one *Socs7* locus. Three targeted ES cell clones were injected into BALB/c blastocysts to generate chimeric mice. Two clones generated germline chimeras, and these were mated with C57BL/6 mice to produce two independent lines (lines 1 and 2) of *Socs7* heterozygotes. The heterozygotes were then interbred to produce wild-type (*Socs7*$^{+/+}$), heterozygous (*Socs7*$^{+/-}$), and homozygous mutant (*Socs7*$^{-/-}$) mice. The genotypes of offspring were routinely determined by Southern blot analysis of *Sac*I-digested genomic DNA extracted from tail biopsies by using the 3′ probe described above (Fig. 1*B*). The predicted targeting

Abbreviations: CSF, colony-stimulating factor; E*n*, embryonic day *n*; P*n*, postnatal day *n*; SCF, stem cell factor; SCO, subcommissural organ; SH2, Src homology 2.

‡To whom correspondence should be addressed. E-mail: alexandw@wehi.edu.au.

www.pnas.org/cgi/doi/10.1073/pnas.0406870101

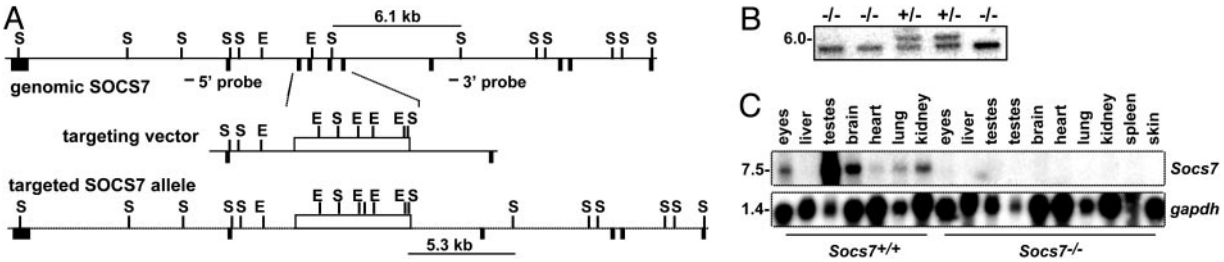

Fig. 1. Disruption of the *Socs7* gene by homologous recombination. (*A*) The endogenous *Socs7* gene is shown, with the *Socs7* coding exons indicated as shaded boxes. The targeting vector was designed such that in the targeted allele four exons are replaced by the β-galactosidase-PGKneo cassette. (*B*) Southern blot of *Sac*I-digested genomic DNA obtained from tail tips of offspring from a cross between $Socs7^{+/-}$ mice. The blot was hybridized with a 3′ genomic *Socs7* probe (indicated in *A*), distinguishing between the endogenous (6.1 kb) and targeted (5.3 kb) alleles. The size in kilobases is indicated at the left. (*C*) Northern blot of RNA obtained from a variety of wild-type and $Socs7^{-/-}$ tissues. The blot was hybridized with a *Socs7* cDNA probe (*Upper*) and then stripped and rehybridized with a *gapdh* cDNA probe (*Lower*) to control for the quality and quantity of mRNA. E, *Eco*RV; S, *Sac*I.

event was also confirmed in Southern blot analyses with a 5′ probe (Fig. 1). All studies were performed on C57BL/6 mice.

Nucleic Acid Analysis. Extraction of genomic DNA from tail tips and analysis by Southern blot were performed as described in ref. 10. Total RNA was extracted from tissues by using TRIzol reagent according to the manufacturer's instructions (Invitrogen). The *Socs7* cDNA probe used for Northern blot hybridization was a 1.3-kb *Eco*RI–*Xho*I fragment. The glyceraldehyde-3-phosphate dehydrogenase (*gapdh*) cDNA probe used for Northern blot analysis was a 1.2-kb *Pst*I fragment. For *in situ* hybridization, a probe containing sequence from position +135 to +1151 of the mouse *Socs7* cDNA was cloned into pBluescript KS, and radiolabeling and hybridizations were performed essentially as described in ref. 11.

Histology. Tissues (uterus, bladder, liver, testes, seminal vesicles, skin, eye, kidney, heart, lung, thymus, salivary gland, small intestine, muscle, spleen, and pancreas) were fixed in 10% buffered formalin and embedded in paraffin. Sections were then prepared, stained with hematoxylin/eosin, and examined by light microscopy. Perfusion-fixed brains, either dissected from the skull or within the skull after decalcification in Jenkin's fluid to maintain the integrity of the hydrocephalic tissue and to allow assessment of the meninges, were processed for paraffin sectioning. Serial sections of brains or brains within the skulls were stained with cresyl violet or hematoxylin/eosin, respectively.

Hematology. Peripheral white blood cell and platelet counts were determined manually by using hemocytometer chambers. Single-cell suspensions from femoral bone marrow, spleen, thymus, and peritoneum were prepared by using standard techniques, and differential cell counts were performed on smears or cytocentrifuge preparations stained with May–Grunwald–Giemsa. Analysis of agar cultures was carried out essentially as described in ref. 12. Briefly, colony formation was stimulated by the addition of granulocyte–macrophage colony-stimulating factor (GM-CSF, 10 ng/ml), macrophage CSF (M-CSF, 10 ng/ml), granulocyte CSF (G-CSF, 10 ng/ml), IL-3 (10 ng/ml), SCF (50 ng/ml), erythropoietin (2 units/ml), thrombopoietin (TPO, 100 ng/ml), IL-6 (500 ng/ml), Flk ligand (500 ng/ml), leukemia inhibitory factor (LIF, 100 ng/ml), or combinations of these cytokines. After 7 days of incubation at 37°C in a humidified atmosphere of 10% CO_2 in air, cultures were fixed and then stained for acetylcholinesterase, Luxol fast blue, and hematoxylin and were examined microscopically to determine the number and composition of colonies. The concentrations of serum creatinine, sodium, bilirubin, potassium, calcium, alkaline phosphatase, chloride, total protein, aspartate aminotransferase, albumin, creatine kinase, urea, and globulin were determined by IDEXX Diagnostic Laboratory (Mount Waverley, Australia).

Flow Cytometry. Single-cell suspensions were prepared from bone marrow, spleen, thymus, mesenteric lymph node, and peritoneal cells from 8- to 12-week-old $Socs7^{-/-}$ mice and wild-type littermates. Erythrocytes were lysed and the cells were stained with rat monoclonal antibodies for specific cell-surface markers and analyzed by flow cytometry as described in ref. 13. Cells were analyzed by using FACStar Plus (Becton Dickinson) excluding dead cells with propidium iodide staining.

Blood Glucose and Serum Insulin. Mice were fasted overnight or fed ad libitum and then bled for total blood or preparation of serum. All blood glucose concentrations were determined by using Advantage glucometer and Advantage II glucose blood test strips (Roche). Plasma insulin concentrations were determined by using the Ultra-sensitive Rat Insulin ELISA kit together with the mouse insulin standard (Crystalchem, Downers Grove, IL).

Results

Disruption of the *Socs7* Gene in Mice. Two lines of mice bearing the disrupted *Socs7* gene were generated from independently targeted ES clones as outlined in *Materials and Methods* and Fig. 1*A*. The majority of analyses were performed on one of these independent $Socs7^{-/-}$ lines (line 1), with key observations confirmed in the second line (line 2). To determine whether *Socs7* was functionally disrupted by this targeting strategy, total RNA was isolated from a panel of wild-type and $Socs7^{-/-}$ tissues and subjected to Northern blot analysis with a cDNA probe containing sequence from exons located in both deleted and undeleted regions of the targeted *Socs7* locus. In wild-type mice, *Socs7* mRNA was expressed primarily in testes and brain, and to a lesser extent in eye and kidney. *Socs7* mRNA was undetectable in all $Socs7^{-/-}$ tissues examined (Fig. 1*C*). Because the deletion created in the targeted *Socs7* allele is distant from the presumed transcriptional regulatory elements at the 5′ end of the gene, the absence of detectable *Socs7* RNA in homozygous mutants seems most likely to be due to instability of any disrupted transcript that might be produced or the interruption of intragenic regulatory sequences. Offspring of heterozygous parents ($n = 292$) included $Socs7^{+/+}$ (27%), $Socs7^{+/-}$ (51%), and $Socs7^{-/-}$ (22%) mice in numbers consistent with normal Mendelian segregation of the targeted *Socs7* allele, suggesting that *Socs7* was not required for embryonic development or survival to weaning. Although $Socs7^{-/-}$ mice appeared grossly normal at birth, between 3–15 weeks of age they began to exhibit lethargy and weight loss accompanied by macrocephalus characterized by a swollen, dome-shaped cranium indicative of hydrocephalus. At this age, ≈50% of $Socs7^{-/-}$ mice became moribund or died. The same

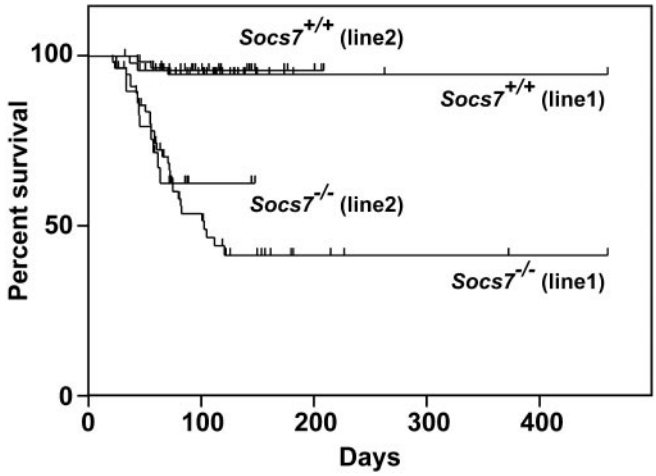

Fig. 2. Mortality in *Socs7*$^{-/-}$ mice. Mice that died or were killed when moribund were included in the analysis. *Socs7*$^{-/-}$ mice from lines 1 ($n = 57$) and 2 ($n = 29$) are plotted separately, with *Socs7*$^{+/+}$ littermates ($n = 60$ and 49, respectively) used as controls for each line. Survival curves were constructed by using PRISM 3 software (GraphPad, San Diego).

pattern of premature death with evidence of hydrocephalus was apparent in both independently derived lines of *Socs7*$^{-/-}$ mice (Fig. 2).

***Socs7*$^{-/-}$ Mice Exhibit a Defect in Cerebrospinal Fluid Homeostasis.** The fact that moribund *Socs7*$^{-/-}$ mice exhibited gross enlargement of the cranium suggested that these mice suffered from hydrocephalus (Fig. 3). Onset occurred from 3–15 weeks of age (60 ± 27 days of age) and was generally accompanied by lethargy and weight loss. A proportion of the *Socs7*$^{-/-}$ mice suffering from hydrocephalus did not exhibit dramatic enlargement of the cranium, but postmortem examination revealed excess acellular ventricular cerebrospinal fluid. Because these animals were older (75 ± 30 days of age) than mice with clearly enlarged crania (48 ± 15 days of age), the lack of cranial enlargement in this group is probably due to the occurrence of hydrocephalus after ossification of the cranial sutures. Surface bleeding was evident in the brains of some affected mice, and fluid was occasionally also observed between the skull and the brain. Brains of six control mice, five *Socs7*$^{-/-}$ mice with overt hydrocephalus, and one *Socs7*$^{-/-}$ mouse without overt hydrocephalus were analyzed histologically. Enlargement of the fluid-filled lateral ventricles was evident only in the five *Socs7*$^{-/-}$ mice with overt hydrocephalus (Fig. 3 *D* and *F*). The cerebral cortex was markedly reduced in thickness, and although cortical layers were still discernable, they were less discrete than in control animals. Other brain areas appeared compressed and displaced caudally. In the more severe cases, the enlargement of the lateral ventricles was accompanied by an enlargement of the fourth ventricle. This finding indicates a patent communication between the lateral and the fourth ventricles via the third ventricle and the aqueduct in a subset of affected animals. Tissue damage ranged from mild to severe with disruption of the septum (Fig. 3*D*), disruption of the transition from the retrosplenial cortex to the hippocampus (Fig. 3*F*), and hemorrhages. However, adhesions in the region of the basal cisterns and subarachnoid hemorrhage were unlikely to have contributed to the development of hydrocephalus because these were not observed in the majority of *Socs7*$^{-/-}$ mice with hydrocephalus. The only specific abnormality detected by histological analysis within the brain was restricted to the subcommissural organ (SCO). The SCO appeared disorganized in all *Socs7*$^{-/-}$ brains, even in the animal without overt hydrocephalus (Fig. 3*H*). Morphological abnormality of

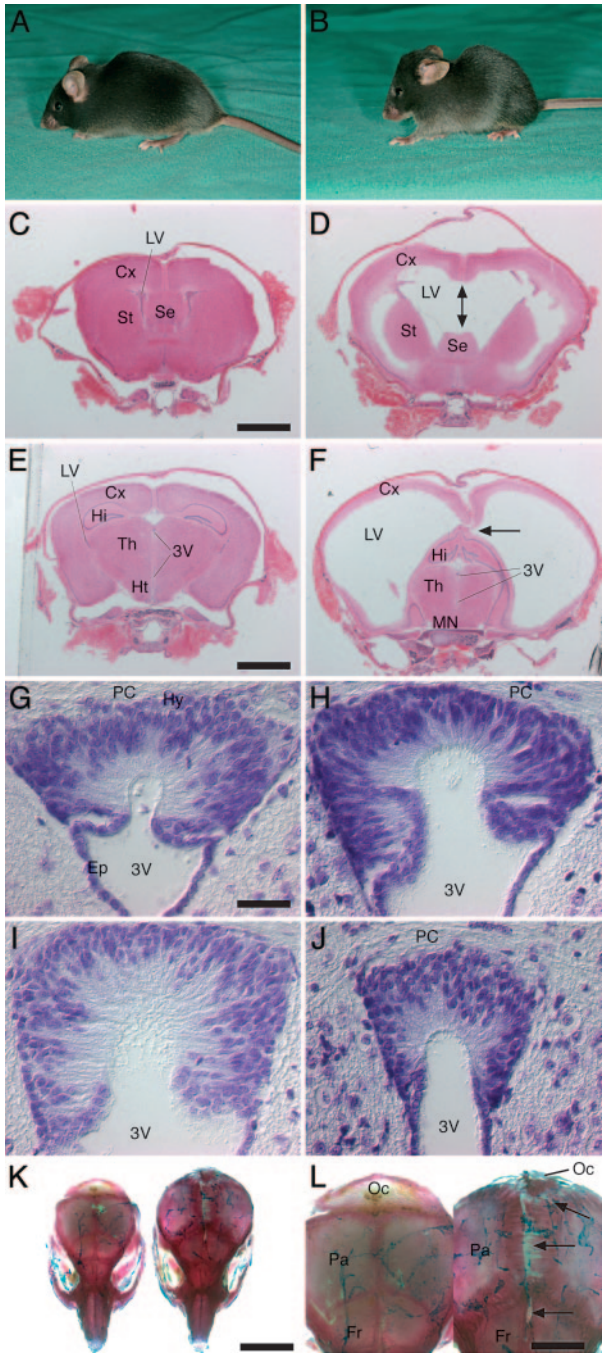

Fig. 3. *Socs7*$^{-/-}$ mutant phenotype. *Socs7*$^{-/-}$ mice were analyzed clinically and pathohistologically for anatomical abnormalities. Images of wild-type or heterozygous controls are shown in *A*, *C*, *E*, *G*, *K Left*, and *L Left*, and images of *Socs7*$^{-/-}$ mutants are shown in *B*, *D*, *F*, *H–J*, *K Right*, and *L Right*. (*A* and *B*) *Socs7*$^{-/-}$ mice exhibited reduced activity, failure to feed, and macrocephalus, suggesting clinically overt hydrocephalus, which was subsequently confirmed by postmortem examination. (*C–F*) Expansion of the fluid-filled lateral ventricles evident in hematoxylin/eosin-stained sections of brains within skulls. Note the disruption of the septum (arrow in *D*) and the retrosplenial cortex to hippocampus transition (arrow in *F*). (*G–J*) Disorganization of the SCO in *Socs7*$^{-/-}$ mutants (*H–J*) compared with the defined structure of the wild-type control (*G*). (*K* and *L*) *Socs7*$^{-/-}$ mutant animals (*Right*) with overt hydrocephalus exhibited a failure of calvarial bone suture closure (arrows), whereas sutures were closed in age-matched controls (*Left*). 3V, third ventricle; Cx, cerebral cortex; Ep, ependyma; Fr, frontal bone; Hi, hippocampus; Ht, hypothalamus; Hy, hypependyma; LV, lateral ventricle; MN, mammillary nuclei; Oc, occipital bone; Pa, parietal bone; PC, posterior commissure; Th, thalamus; Se, septum; St, striatum. (Scale bars: *C* and *D*, 2 mm; *E* and *F*, 2.3 mm; *G–J*, 40 μm; *K*, 7.1 mm; *L*, 4.4 mm.)

Table 1. Hematological profile of *Socs7*$^{-/-}$ mice

Parameter	*Socs7*$^{-/-}$	*Socs7*$^{+/+}$
Peripheral blood platelets, $\times 10^{-6}$/ml	929 ± 196	909 ± 159
Hematocrit, %	44 ± 2	45 ± 3
White blood cell count, $\times$ 10^{-6}/ml	9.3 ± 3.7	6.8 ± 1.9
Neutrophils	1.3 ± 0.5	0.5 ± 0.2
Lymphocytes	6.9 ± 3.3	5.9 ± 1.7
Monocytes	0.9 ± 0.5	0.4 ± 0.2
Eosinophils	0.2 ± 0.2	0.05 ± 0.06

Mean ± SD of data from seven to eight mice of each genotype.

the SCO seemed to progress with the development of hydrocephalus (Fig. 3 *I* and *J*). Analysis of serial sections did not reveal any other structural abnormality within the brain, including the choroid plexus, the meninges, or the skull, that could account for a stasis in cerebrospinal fluid flow.

Animals exhibiting overt hydrocephalus showed calvarial bone suture fusion defects between the parietal, frontal, and occipital bones, presumably secondary to the enlargement of the brain before physiological closure of the sutures (Fig. 3 *K* and *L*). The foramen magnum was of normal size.

Although C57BL/6 mice are known to develop hydrocephalus at relatively high frequency among inbred laboratory mouse strains, the incidence is only 1–3% (14). Consistent with these data, we found that only two *Socs7*$^{+/-}$ and one *Socs7*$^{+/+}$ mice developed hydrocephalus in our colony of several hundred animals, an incidence clearly insignificant in comparison with the onset in *Socs7*$^{-/-}$ mice.

Mild Growth Retardation in *Socs7*$^{-/-}$ Mice. Histological analysis of an additional 16 tissues from each of 19 moribund *Socs7*$^{-/-}$ mice sampled from both independent lines and 13 healthy age-matched *Socs7*$^{+/+}$ controls revealed that there were no additional abnormalities in *Socs7*$^{-/-}$ tissues, with the exception of the pancreas (see below). In addition, biochemical analysis of *Socs7*$^{-/-}$ serum to investigate possible liver, heart, muscle, kidney, bone, and pancreas abnormalities (see *Materials and Methods*) did not reveal irregularities (data not shown). However, during the histological analysis it became apparent that *Socs7*$^{-/-}$ organs were smaller in size than those of their wild-type counterparts. By weighing individual organs, a uniform diminution in size of all *Socs7*$^{-/-}$ tissues of ≈10% was observed (data not shown). To formally examine the growth of *Socs7*$^{-/-}$ mice, offspring from *Socs7*$^{+/-}$ crosses were weighed weekly from weaning until 14 weeks of age. In agreement with reduced organ size, *Socs7*$^{-/-}$ male and female mice weighed 7–10% less than their sex-matched *Socs7*$^{+/+}$ or *Socs7*$^{+/-}$ littermates at each week from 4 to 14 weeks of age. Growth retardation was also apparent in the second line of *Socs7*$^{-/-}$ mice; however, in this case the difference was not statistically significant at all ages (data not shown).

Hematological Parameters in *Socs7*$^{-/-}$ Mice. The hematocrit, the number of circulating platelets, and the numbers and proportions of specific white blood cells were within the normal ranges in *Socs7*$^{-/-}$ mice, although a minor but consistent elevation in neutrophil numbers was evident (Table 1). The frequencies of morphologically recognizable cell types in the peritoneal cavity, bone marrow, and spleen were also normal, and fluorescence-activated cell sorting analysis of the thymus, spleen, mesenteric node, and bone marrow confirmed that there were no anomalies in the frequency of T and B lymphocytes, macrophages, granulocytes, or erythroid cells in *Socs7*$^{-/-}$ tissues (data not shown). There was no perturbation in *Socs7*$^{-/-}$ mice in the number and

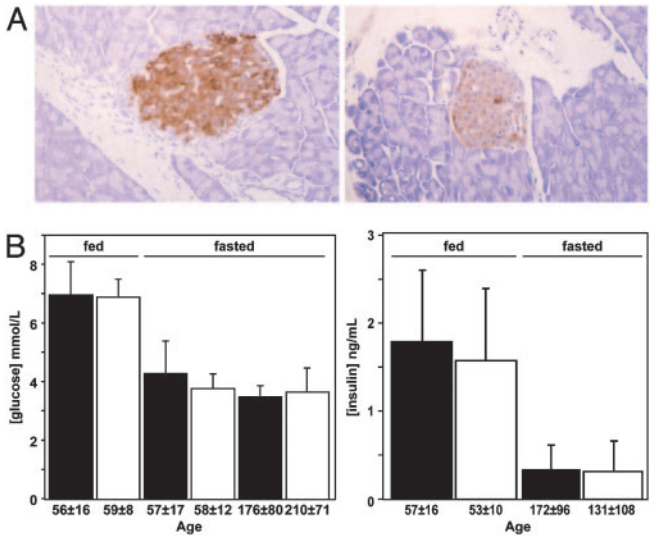

Fig. 4. Glucose homeostasis in *Socs7*$^{+/+}$ and *Socs7*$^{-/-}$ mice. (*A*) Histological sections of *Socs7*$^{-/-}$ (*Left*) and *Socs7*$^{+/+}$ (*Right*) pancreas showing more intense insulin staining in an islet of Langerhans in the *Socs7*$^{-/-}$ mouse. (*B*) Blood glucose (*Left*) and serum insulin (*Right*) levels were determined for *Socs7*$^{+/+}$ (open bars) or *Socs7*$^{-/-}$ (filled bars) mice that were either fasted overnight or fed ad libitum (n = 7–13). Age (mean ± SD) is shown at bottom.

lineage commitment of committed hematopoietic progenitor cells responsive to GM-CSF, G-CSF, M-CSF, IL-3, erythropoietin, SCF, TPO, or IL-6, and the synergistic response to the combination of SCF plus IL-3 plus erythropoietin was intact. Blast colony formation in response to IL-3, SCF, or the combinations SCF plus G-CSF and Flk ligand plus LIF were also normal (data not shown).

Glucose Homeostasis in *Socs7*$^{-/-}$ Mice. An observation in some *Socs7*$^{-/-}$ mice was the presence of unusually large islets of Langerhans in the pancreas, and, unrelated to size, *Socs7*$^{-/-}$ islets showed particularly intense and uniform staining for insulin in seven of nine mice examined with comparable staining observed in only one of seven *Socs7*$^{+/+}$ mice (Fig. 4). To investigate glucose homeostasis, we measured blood glucose and serum insulin levels in fasted and fed *Socs7*$^{-/-}$ and *Socs7*$^{+/+}$ littermates. We found that *Socs7*$^{-/-}$ mice were indistinguishable from their wild-type counterparts with respect to these parameters (Fig. 4).

Expression of the *Socs7* Gene. The expression pattern of the *Socs7* gene was examined by *in situ* hybridization at embryonic day (E) 12.5, E15.5, postnatal day (P) 7, P14, and P21 spanning the time of development of the overt hydrocephalus in *Socs7*$^{-/-}$ mice. Sagittal sections of embryos at E12.5 and E15.5 showed very low-level ubiquitous expression of *Socs7* mRNA, just above background levels of a sense control probe. Only the nervous system at E12.5 (telencephalon shown in Fig. 5*A*) and the cortical plate at E15.5 exhibited moderately high levels of *Socs7* mRNA (Fig. 5*C*). The *Socs7* gene continued to be expressed in the brain at postnatal stages, showing higher levels of expression in the hippocampal formation and in the medial habenular nuclei (P7 shown in Fig. 5*E*). Low-level expression in other brain areas was present at P7 and was reduced to very low levels at P14 and P21. The hippocampal granule cell layer and the cerebellar granular layer maintained moderate expression levels at P7, P14, and P21. Moderate levels of *Socs7* mRNA in the E15.5 cortical plate, postnatal hippocampal granule cells, and the cerebellar granular layer indicated *Socs7* expression in neurons but did not exclude

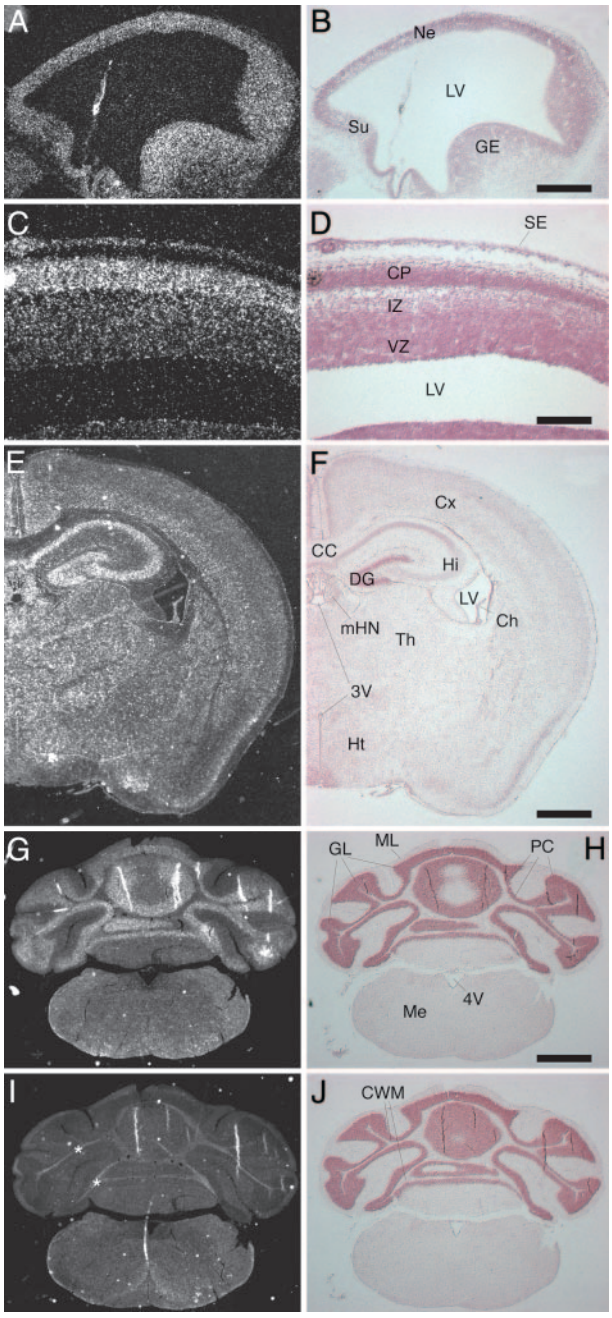

Fig. 5. Expression pattern of the *Socs7* gene. Expression of *Socs7* mRNA was analyzed by radioactive *in situ* hybridization with a *Socs7*-specific [^{35}S]UTP-labeled cRNA probe. Silver grains represent the location of *Socs7* mRNA shown in dark-field images (*A*, *C*, *E*, *G*, and *I*; the corresponding bright-field images are depicted in *B*, *D*, *F*, *H*, and *J*). (*A* and *B*) Moderately high levels of expression were observed in E12.5 telencephalon. (*C* and *D*) E15.5 fetuses showed moderately high levels of *Socs7* mRNA expression in the cortical plate and the overlying surface ectoderm. (*E* and *F*) P7 brain exhibited low-level widespread expression with moderately high levels of expression in the hippocampus and the medial habenular nuclei. (*G* and *H*) *Socs7* was moderately expressed in the granular layer of the P21 cerebellum. (*I* and *J*) Sense control probe. Nonspecific reflection of light from the cerebellar white matter is evident (*). 3V, third ventricle; 4V, fourth ventricle; Ch, choroid plexus; CC, corpus callosum; CP, cortical plate; CWM, cerebellar white matter; Cx, cerebral cortex; DG, dentate gyrus; GE, ganglionic eminence; GL, granular layer; Hi, hippocampus; Ht, hypothalamus; IZ intermediate zone; LV, lateral ventricle; Me, medulla; mHN, medial habenular nuclei; ML, molecular layer; Ne, neocortical neuroepithelium; PC, Purkinje cell layer; SE surface ectoderm; Su, subiculum; Th, thalamus; VZ, ventricular zone. (Scale bars: *A* and *B*, 320 μm; *C* and *D*, 160 μm; *E* and *F*, 800 μm; *G–J*, 1.1 mm.)

expression in astrocytes. Other brain areas including the choroid plexus at E15.5, P7, P14, and P21 exhibited low to very low levels of *Socs7* mRNA.

In situ hybridization also revealed strong *Socs7* gene expression in adult testes, specifically in spermatocytes and early spermatids. Levels of *Socs7* mRNA in spermatogonia, maturing spermatids, Sertoli cells, and Leydig cells were very low (data not shown). Despite this expression pattern, no histological abnormalities were noted in *Socs7*$^{-/-}$ testes, and sperm isolated from these mice exhibited normal morphology, motility, capacitation, and fertility (data not shown).

Discussion

To investigate the biological action of SOCS7, we have used homologous recombination in ES cells to generate mice that lack expression of the *Socs7* gene. *Socs7*$^{-/-}$ mice were born in numbers consistent with a normal Mendelian pattern of inheritance of the targeted allele, were fertile, and did not exhibit alterations in serum biochemistry or gross organ morphology, excepting that of the brain. Previous studies had implicated SOCS7 and/or its most closely related SOCS family member, SOCS6, in the regulation of SCF and insulin signaling (5–7). To address the possibility that SOCS7 might regulate these signaling pathways, we investigated hematopoiesis and glucose homeostasis in *Socs7*$^{-/-}$ mice. We could not detect anomalies in the frequency or lineage commitment of hemopoietic progenitor cells or in the morphology or total number of hemopoietic cells in the periphery, spleen, bone marrow, or peritoneal cavity of *Socs7*$^{-/-}$ mice. Responses of hematopoietic progenitor cells to stimulation with SCF *in vitro* were also normal.

Previous studies have shown that manipulation of insulin regulation can influence body weight (15). Thus, given that SOCS7 can bind several proteins implicated in insulin signaling, an obvious hypothesis was that that the mild growth retardation evident in *Socs7*$^{-/-}$ mice may reflect altered insulin and/or glucose homeostasis. Indeed, in some *Socs7*$^{-/-}$ mice the pancreatic islets of Langerhans were often unusually large, and many islets, independent of size, exhibited stronger staining for insulin than apparent in *Socs7*$^{+/+}$ islets. However, measurements of both circulating insulin and glucose in *Socs7*$^{-/-}$ mice revealed no abnormalities. Interestingly, SOCS6 interacts with a similar set of insulin signaling regulators, and *Socs6*$^{-/-}$ mice also exhibit mild growth retardation. However, like *Socs7*$^{-/-}$ mice, mice lacking SOCS6 also failed to exhibit any obvious anomaly in glucose or insulin homeostasis (4). It remains possible that these mutants have subtle alterations in insulin signaling that more extensive analyses may reveal. Moreover, the similarities in sequence between SOCS6 and SOCS7, their shared SH2 domain binding specificities, and the similar mild growth defect in mice deficient in either of these proteins makes a compelling case for functional redundancy between SOCS6 and SOCS7. Analysis of insulin and glucose homeostasis in mice lacking both *Socs6* and *Socs7* may therefore be particularly revealing.

At birth, *Socs7*$^{-/-}$ mice appeared grossly normal, but between 3–15 weeks of age approximately half of these mice developed fatal hydrocephalus. No expansion of brain tissue or abnormalities of the choroid plexus, the meninges, or the skull were detected upon histological examination that could account for the development of hydrocephalus. The only structural abnormality observed was the disorganization of the SCO. The SCO is situated at the forebrain–midbrain boundary at the transition between the third ventricle and the aqueduct. The SCO secretes glycoproteins into the cerebrospinal fluid (16). Although the function of the SCO remains unclear, the SCO has been implicated in the pathogenesis of hydrocephalus because the absence or dysgenesis of the SCO has been associated with the development of this disorder in rat and mouse mutants. Although it is conceivable that disorganization of the SCO is a consequence

rather than a cause of hydrocephalus, in some cases the absence or dysgenesis of the SCO precedes the development of hydrocephalus (17–19). Indeed, disorganization of the SCO was present in a *Socs7*$^{-/-}$ animal without hydrocephalus and was more pronounced in animals with overt hydrocephalus. These data can be interpreted in two ways. Firstly, the structure of the SCO may be directly affected by the lack of *Socs7*, and this defect is simply exacerbated by increased intracerebral pressure due to hydrocephalus. Alternatively, the disorganization of the SCO caused by *Socs7* may be related causally to the development of hydrocephalus. Although the data here cannot distinguish these possibilities, the latter hypothesis may be supported by the absence of other structural abnormalities in the *Socs7*$^{-/-}$ brains. However, alternative mechanisms leading to hydrocephalus that may not be evident upon histological examination are also feasible, including dysfunction of the choroid plexus or the lymphatic and vascular drainage from the subarachnoid space.

Hydrocephalus associated with morbidity and mortality was observed with only 40–60% incidence in *Socs7*$^{-/-}$ mice, suggesting that the *Socs7*$^{-/-}$ mutant phenotype occurs with incomplete penetrance. Although this is clearly the case for the severe hydrocephalus, it remains possible that consistent anomalies occur more frequently in *Socs7*$^{-/-}$ brains, resulting in overt defects in only a subset of mice. Given the inbred genetic background of these studies, the incomplete penetrance of hydrocephalus may be contributed to by functional redundancy of *Socs7* with other SOCS proteins. As outlined for insulin homeostasis above, the most likely candidate for redundancy with *Socs7* is its most similar relative, *Socs6*. It is noteworthy that, like *Socs7*, *Socs6* is expressed prominently in the brain (4), although the precise locations of *Socs6* expression in this organ are not known. A deeper understanding of the comparative expression patterns of *Socs6* and *Socs7*, along with the generation of mice deficient in both *Socs6* and *Socs7*, will be important in revealing the redundant actions of these SOCS family members in the brain and may uncover other physiological actions of SOCS6 and SOCS7.

We acknowledge the excellent animal husbandry of Katya Gray and Kelly Trueman and the technical assistance of Amy Herlihy. This work was supported by National Health and Medical Research Council, Canberra, Program Grant 257500; the Anti-Cancer Council of Victoria; the J. D. and L. Harris Trust; and the Australian Federal Government Cooperative Research Centres Program.

1. Krebs, D. L. & Hilton, D. J. (2000) *J. Cell Sci.* **113,** 2813–2819.
2. Starr, R., Willson, T. A., Viney, E. M., Murray, L. J., Rayner, J. R., Jenkins, B. J., Gonda, T. J., Alexander, W. S., Metcalf, D., Nicola, N. A. & Hilton, D. J. (1997) *Nature* **387,** 917–921.
3. Matuoka, K., Miki, H., Takahashi, K. & Takenawa, T. (1997) *Biochem. Biophys. Res. Commun.* **239,** 488–492.
4. Krebs, D. L., Uren, R. T., Metcalf, D., Rakar, S., Zhang, J. G., Starr, R., De Souza, D. P., Hanzinikolas, K., Eyles, J., Connolly, L. M., *et al.* (2002) *Mol. Cell. Biol.* **22,** 4567–4578.
5. Mooney, R. A., Senn, J., Cameron, S., Inamdar, N., Boivin, L. M., Shang, Y. & Furlanetto, R. W. (2001) *J. Biol. Chem.* **276,** 25889–25893.
6. Li, L., Gronning, L. M., Anderson, P. O., Li, S., Edvarsen, K., Johnston, J., Kioussis, D., Shepherd, P. R. & Wang, P. (2004) *J. Biol. Chem.* **279,** 34107–34114.
7. Bayle, J., Letard, S., Frank, R., Dubreuil, P. & De Sepulveda, P. (2004) *J. Biol. Chem.* **279,** 12249–12259.
8. Martens, N., Wery, M., Wang, P., Braet, F., Gertler, A., Hooghe, R., Vandenhaute, J. & Hooghe-Peters, E. L. (2004) *Exp. Cell Res.* **298,** 239–248.
9. Kontgen, F., Suss, G., Stewart, C., Steinmetz, M. & Bluethmann, H. (1993) *Int. Immunol.* **5,** 957–964.
10. Alexander, W. S., Metcalf, D. & Dunn, A. R. (1995) *EMBO J.* **14,** 5569–5578.
11. Thomas, T., Voss, A. K., Chowdhury, K. & Gruss, P. (2000) *Development (Cambridge, U.K.)* **127,** 2537–2548.
12. Kile, B. T., Metcalf, D., Mifsud, S., DiRago, L., Nicola, N. A., Hilton, D. J. & Alexander, W. S. (2001) *Mol. Cell. Biol.* **21,** 6189–6197.
13. Alexander, W. S., Roberts, A. W., Nicola, N. A., Li, R. & Metcalf, D. (1996) *Blood* **87,** 2162–2170.
14. Dagg, C. (1966) in *Biology of the Laboratory Mouse*, ed. Green, E. (McGraw–Hill, New York), pp. 309–328.
15. Woods, S. C., Seeley, R. J., Porte, D., Jr., & Schwartz, M. W. (1998) *Science* **280,** 1378–1383.
16. Rodriguez, E. M., Rodriguez, S. & Hein, S. (1998) *Microsc. Res. Tech.* **41,** 98–123.
17. Louvi, A. & Wassef, M. (2000) *Development (Cambridge, U.K.)* **127,** 4061–4071.
18. Bach, A., Lallemand, Y., Nicola, M. A., Ramos, C., Mathis, L., Maufras, M. & Robert, B. (2003) *Development (Cambridge, U.K.)* **130,** 4025–4036.
19. Blackshear, P. J., Graves, J. P., Stumpo, D. J., Cobos, I., Rubenstein, J. L. & Zeldin, D. C. (2003) *Development (Cambridge, U.K.)* **130,** 4539–4552.